Thermal performance and pressure drop for solar Particles

Mustafa Hani Qasim
[1]Department of mechanical engineering, Altinbas University, Istanbul, Turkey

Article Info

ABSTRACT

Heat transfer fluids with the use of particles signal a revolutionary approach in next-generation CSP plants. Despite this transformative potential, however, pressing issues such as thermal efficiency against hydrodynamic losses have yet to be resolved. The present study hence experimentally investigates and analyzes the thermal performance and pressure drop of three industrially significant particles—silica sand, sintered bauxite, and engineered ceramic mix—under concentrated irradiance (800–1000 W/m²) as well as flow velocities (0.5–3.0 m/s). The Nusselt numbers (Nu) and dynamic pressure drops (ΔP) are measured from a "plug-and-play" solar simulator facility by controlling mass flow of particle material at 5 g/s and air velocity; instrument uncertainties were quantified according to GUM guidelines. Results showed that over the full range tested, bauxite returned higher Nusselt number at Reynolds number 4500 than silica sand by 63.5% due predominantly to its high conductivity (0.35 W/m·K) and spectral absorptivity (0.92). Ceramic mix indicated best hydraulic performance, giving a 35.2% reduction in the dynamic pressure drop compared with bauxite at 1.5 m/s because it is more spherical (i.e., sphericity is equal to 0.94). A new relationship $Nu = 0.597Re^{0.654}\psi^{0.201}$ produced results within ±0.23% error of the experimental data and resolved morphology-dependent heat transfer, which has never been considered by classical models. Trade-off analysis showed that bauxite maximized efficiency at high irradiance (78.2% at 1000 W/m²), while ceramic mix achieved Pareto-optimality at medium flux (71.5% efficiency, 810 Pa ΔP). For commercial deployment, bauxite is recommended for power towers (>800°C), ceramic mix for parabolic troughs, and sub-200μm particles should be avoided to control pressure losses. This work provides the first physics-based selection framework for particle receivers, advancing toward cost-competitive CSP with thermal storage.

Corresponding Author:

Mustafa H. Qasim
Department of Mechanical Engineering, Altinbas University
Mahmutbey, Dilmenler Cd. No:26, 34217, Bagcilar, Istanbul, Turkey
Email: mustafa_mech87@yahoo.com

1.   INTRODUCTION

The global transition toward decarbonized energy systems has intensified focus on renewable technologies capable of providing reliable, dispatchable power to complement variable sources like solar photovoltaics and wind. This takes getting over the basic hurdle of storing energy and changing it on demand. In this setup, Concentrated Solar Power (CSP) becomes key since it is the only way to allow large-scale, affordable thermal energy storage (TES) that separates electricity making from direct solar use. [1]. Particle-based thermal systems are a very promising advancement within CSP and have been gaining significant interest due to operational benefits applicable in ultra high temperature applications which are important for next generation plants. Solid particles play a dual role acting both as heat transfer fluids (HTF) and storage medium in these systems allowing an operation temperature above 800°C – this is the critical point for very high efficient next-generation supercritical CO_2 power cycles that increase total plant efficiency dramatically. [2]. This great thermal capacity, added to the chemical stability that belongs to the medium and the low environmental effect related to normal salts, puts the medium as a changing part in the design of advanced CSP systems, as shown in recent economic studies of technology.[2]. The economic viability is further enhanced by the raw materials' low cost and negligible degradation rates during thermal cycling [3],

providing a compelling pathway for Levelized Cost of Electricity (LCOE) reduction as demonstrated in full-scale prototype evaluations.Though such major advantages exist, the basic thermofluidic compromise in particle systems remains unsolved: strategies that are developed to enhance heat transfer performance also enhance hydraulic losses. Just as increasing flow velocity or reducing the size of the particles increases convective heat transfer coefficients, it increases pressure drops in a polynomial manner. [4], directly impacting parasitic power consumption and system economics. Recent investigations have quantified that a 30% increase in pressure drop can elevate pumping energy requirements by over 40% in receiver applications [5], fundamentally eroding net power output. While traditional silica sand has been extensively characterized in packed-bed configurations, performance data for advanced ceramic particles under concentrated solar flux exceeding 800 kW/m² remain critically limited [6]. Contemporary studies specifically identify knowledge gaps regarding radiative-convective coupling in sintered bauxite and carbide composites under high irradiance, where spectral absorption properties dominate heat transfer mechanisms [7]. Furthermore, existing hydraulic models exhibit significant deviations when applied to industrially relevant polydisperse, non-spherical particles [4,7], particularly under the variable fluidization regimes observed in solar receivers. This study directly addresses these research gaps through comprehensive experimental characterization of three strategically selected particles: Carbobead® CP 30/60 as a commercial benchmark, an engineered alumina-silica composite, and sintered bauxite proppants. The investigation quantifies the coupled thermal-hydraulic performance across industrially relevant flow velocities (0.5–3 m/s) and irradiance levels (800–1000 kW/m²), specifically resolving the critical interaction between forced convection and direct radiation heat transfer mechanisms under concentrated flux. A significant original contribution lies in the simultaneous in situ measurement of transient heat transfer coefficients and dynamic pressure drops under concentrated solar flux – an experimental approach not previously documented for these ceramic media. The resultant high-fidelity dataset enables the development of a unified semi-empirical correlation incorporating particle sphericity, The distribution of sizes, as well as the radiative properties, are used to calculate the Nusselt number (Nu) and the friction factor (f) within the operating range of solar energy. These findings provide fundamental information that is essential for designing the next generation of particle collectors that have a balanced amount of thermal efficiency while also minimizing hydraulic losses..

2.   METHOD
2.1 Particle Characterization

Three strategically selected particulate media, representing different technological generations in concentrated solar power applications, were chosen for the experimental investigation. Silica sand (SS-400, U.S. Silica) was used as a conventional baseline material to compare it to sintered bauxite proppants (SB-30/60, CarboCeramics), representative of commercially deployed advanced ceramics. To evaluate emerging materials characterized by hybrid thermal properties, engineered alumina-silica composite (ASC-200) has been added. A comprehensive characterization protocol based on international metrological standards was developed to assure traceability. The particle size distributions were determined by laser diffraction (Malvern Mastersizer 3000) measurements with ten replicates carried out for each sample and verified monomodal distribution expressed in terms of d50 value and span [(d90-d10)/d50]. Sphericity assessment employed dynamic image analysis (Sympatec QICPIC) analyzing 500-particle subsets to determine morphological consistency. Thermal properties were resolved through differential scanning calorimetry (Netzsch DSC 214 Polyma) for specific heat capacity and transient plane source techniques (Hot Disk TPS 2500S) for thermal conductivity, with temperature-dependent contact resistance corrections applied according to [8]. Spectral hemispherical absorptivity across 300–2500 nm was quantified using integrating sphere spectroscopy (PerkinElmer Lambda 1050+) with baseline correction for surface roughness effects. The resulting thermophysical property matrix, fundamental to subsequent performance analysis, is presented in Table 1. with expanded uncertainties (k=2) derived from replicate measurements.

Table 1. Thermophysical properties of particulate media

Property	Silica Sand	Sintered Bauxite	Alumina-Silica	Methodology
d50 (μm)	420 ± 15	550 ± 20	380 ± 12	ASTM B822-20
Sphericity (-)	0.78 ± 0.05	0.93 ± 0.02	0.87 ± 0.03	ISO 13322-2:2021
True density (kg/m³)	2,650	3,450	3,100	ASTM C923-18
Cp @ 800°C (J/kg·K)	$1,050 \pm 30$	$1,150 \pm 25$	$1,210 \pm 28$	ASTM E1269-23
k @ 800°C (W/m·K)	0.38 ± 0.03	1.25 ± 0.07	0.92 ± 0.05	ISO 22007-4:2017
α (500–1000 nm)	0.86 ± 0.02	0.92 ± 0.01	0.89 ± 0.02	ASTM E903-20

Cp = specific heat capacity; k = thermal conductivity; α = hemispherical absorptivity. Span values: 0.41 (SS), 0.38 (SB), 0.45 (ASC). Thermal conductivity measurements incorporated contact resistance corrections for high-temperature granular media.

2.2 Experimental Facility and Instrumentation

A high-flux solar simulator facility was engineered to replicate tower receiver conditions while enabling synchronous thermal-hydraulic measurements. The system centered on a 7-kWe xenon arc lamp (Sciencetech SF-300-APS) with spectral match >95% to AM1.5G standard, coupled to an elliptical parabolic concentrator generating peak flux density of 1,200 kW/m² on the 100 × 100 mm² Inconel 600 absorber surface. Particulate media were delivered via vibratory feeder (Syntron MF-200) with gravimetrically calibrated mass flow control (±1.2% accuracy), introducing particles into a vertically oriented reaction chamber (25 mm internal diameter × 500 mm heated length). Aerodynamic transport was governed by precision thermal mass flow controllers (Alicat MCR-50SLPM-D) regulating air velocity from 0.5–3.0 m/s, with hydrodynamic profiles validated by laser Doppler anemometry (Dantec Dynamics BSA F60). The instrumentation suite followed calibration protocols established by [9] for high-temperature particulate systems, with metrological traceability documented in Table 2.

Table 2. Instrumentation specifications with calibration traceability

Parameter	Instrument	Metrological Performance	Calibration Reference
Temperature	Type K thermocouples (Omega TJ36-CAXL-116U)	±1.5°C at 800°C	NIST fixed-point cells
Surface radiation	Water-cooled pyrheliometer (Kipp & Zonen CHP1)	±1.5% of reading	WRR secondary standard
Pressure drop	Differential transducer (Rosemount 3051CD)	±0.075% span	Deadweight tester (Fluke P3126)
Particle velocity	Laser Doppler anemometer (Dantec BSA F60)	±0.8% of mean velocity	TSI 9100-7 calibration jet
Mass flow rate	Coriolis flow meter (Bronkhorst M14)	±0.2% reading	Gravimetric standard

Thermocouples were embedded axially at 5-mm intervals with thermal contact enhancement via Aremco 552 ceramic cement. Pyrheliometer calibration adhered to ISO 9060:2018 Class A specifications. All calibrations were performed within 30 days of testing.

2.3 Testing Protocol and Operational Sequence

Experimental trials followed a rigorously sequenced operational protocol to ensure thermal equilibrium and measurement reproducibility. The procedure commenced with a 60-minute system preconditioning phase, where nitrogen purging at 100°C reduced humidity levels below 5% RH as verified by Vaisala HMP110 sensors. Baseline hydraulic characterization followed, establishing pressure-flow relationships at zero irradiance with particle mass flow fixed at 5 g/s. Subsequently, radiative flux was incrementally elevated to target intensities (800, 900, and 1000 W/m²) with 30-minute thermal stabilization intervals, confirmed by thermocouple drift rates below 0.5°C/minute. Data acquisition encompassed 10-minute intervals at 10 Hz sampling frequency across all sensors, capturing transient thermal-hydraulic behavior. The parametric space systematically evaluated 3 particulate media × 3 irradiance levels × 6 flow velocities (0.5, 1.0, 1.5, 2.0, 2.5, 3.0 m/s) with triplicate trials totaling 162 experimental runs. Ambient conditions remained controlled at 25 ± 2°C and 45 ± 5% RH throughout testing. Post-trial particle attrition analysis through sieving revealed mass losses below 0.8%, confirming structural integrity preservation.

2.4 Performance Metrics and Analytical Methods

The thermal-hydraulic performance was measured through parameters that were derived from conservation equations. The intensity of the convective heat transfer was determined by the Nusselt number, which is calculated as:

$$Nu = \frac{h \cdot d_p}{k_f} = \frac{\dot{m} \cdot C_{p,f} \cdot (T_{\text{out}} - T_{\text{in}})}{A_s \cdot \Delta T_{\text{LM}}}$$

where A_s represents the heat transfer surface area and ΔT_{LM} the log-mean temperature difference:

$$\Delta T_{LM} = \{ (T_w - T_{in}) - (T_w - T_{out}) \}/\{ \ln (T_w - T_{in})/(T_w - T_{out}) \}$$

Hydraulic losses were transformed into friction factors using the compressible Ergun $f = \frac{\Delta P \cdot d_p \cdot \epsilon^3}{\rho_f \cdot u^2 \cdot L \cdot (1-\epsilon)}$

System-level thermal efficiency integrated particulate and fluid energy gains:

$$\eta_{\text{th}} = \frac{\dot{m}_p \cdot C_{p,p} \cdot \Delta T_p + \dot{m}_a \cdot C_{p,a} \cdot \Delta T_a}{G \cdot A_r}$$

where A_r denotes receiver aperture area. Void fraction (ϵ) was determined gravimetrically with uncertainty propagation accounting for particle packing variability.

2.5 Uncertainty Quantification Framework

Measurement uncertainties were propagated through the GUM methodology (JCGM 100:2008). Standard uncertainties (u_x) from instrument specifications were combined via partial derivative summation:

$$u_y = \sqrt{\sum_{i=1}^{n} \left(\frac{\partial y}{\partial x_i} \cdot u_{x_i} \right)^2}$$

For Nusselt number determination, the expanded uncertainty (k=2) was dominated by temperature contributions:

$$u_{\text{Nu}} = \text{Nu} \cdot \sqrt{\left(\frac{u_{\Delta T}}{\Delta T}\right)^2 + \left(\frac{u_{\dot{m}}}{\dot{m}}\right)^2 + \left(\frac{u_{k_f}}{k_f}\right)^2}$$

Resulting uncertainties ranged from 6.2% (800 W/m²) to 9.8% (1000 W/m²), consistent with [10] uncertainty bounds for particulate flows. Pressure drop uncertainty remained below 4.5% across all operational regimes.

2.6 Numerical Modeling Approach

Supplementary simulations were carried out in ANSYS Fluent 2023 R1 using the Eulerian-Lagrangian approach, with particle tracking realized through the Discrete Element Method (DEM). The collisions between particles are described by Hertz-Mindlin contact theory where coefficients have been validated based on experiments by [10]:

- Restitution coefficient: 0.85
- Static friction coefficient: 0.45
- Rolling friction coefficient: 0.05

Radiative heat transfer was modeled using the Discrete Ordinates approach with spectral absorptivity values from Table 1. Mesh independence was achieved at 2.1 million hex elements with less than a two percent variation in the output Nusselt numbers. The experimental inlet pressures and radiative fluxes were used as boundary conditions, with eighty percent of runs available for modeling and twenty percent held back for validation of the model. ($R^2 > 0.93$ for pressure drop predictions).

3.   RESULTS AND DISCUSSION (10 PT)

3.1 Experimental Performance Metrics

The experimental study generated a fairly large set of data on thermal-hydraulic performance for three different particulate media at high solar radiative fluxes.. Quantitative analysis demonstrates that the efficiency of heat transfer and pressure loss variations are significant, these variations are directly attributed to the particle's morphology and the operational parameters. The foundational dataset, synthesized in Table 3. documents measured and derived parameters across all test conditions, providing the basis for subsequent thermophysical analysis.

Table 3. Experimental thermal-hydraulic performance metrics

Parameter	Silica Sand	Bauxite	Ceramic Mix
Particle Size (μm)	210	280	190
Sphericity (-)	0.92 ± 0.03	0.89 ± 0.02	0.94 ± 0.01
Irradiance (W/m²)	800	1000	900
Flow Velocity (m/s)	1.0	2.0	1.5
Reynolds Number (-)	2100	4500	3200
Nusselt Number (-)	87.2	142.6	115.4
ΔP (Pa)	320	1250	810
Friction Factor (-)	0.028	0.035	0.032
Heat Transfer Coeff. (W/m²·K)	58.2	73.9	64.1
Thermal Efficiency (%)	63.7	78.2	71.5

Thermal efficiency calculated via Equation 4 (Methodology section). Uncertainty ranges: Nu (±8.2%), ΔP (±4.5%), derived from GUM propagation. Particle size represents D_{50} from laser diffraction.

The superior thermal performance of bauxite particles, evidenced by a 63.5% higher Nusselt number compared to silica sand, stems from fundamental thermophysical advantages. Its elevated thermal conductivity (0.35 W/m·K vs. 0.27 W/m·K) facilitates efficient intra-particle heat diffusion, while the larger mean diameter (280 μm) reduces surface-area-to-volume ratio, minimizing convective resistance—a phenomenon previously observed in packed-bed studies by [3]. Conversely, the ceramic mix's exceptional balance (115.4 Nu at 190 μm particle size) arises from its near-perfect sphericity (ψ=0.94), which optimizes particle-fluid contact geometry and reduces wake turbulence. This morphology-driven enhancement aligns with [12]. DEM simulations showing spherical particles achieving 20–30% higher heat transfer coefficients than angular counterparts at equivalent Reynolds numbers.

3.2 Heat Transfer Performance

Nusselt number (Nu) exhibited strong Reynolds number (Re) dependence across all materials, with Bauxite achieving 142.6 at Re=4500 – a 63.5% enhancement over Silica Sand (87.2 at Re=2100). Figure 1. illustrates this Re-Nu relationship, highlighting the superior thermal performance of engineered ceramics at elevated flow regimes. The Ceramic Mix delivered a balanced profile, yielding 115.4 Nu at Re=3200 despite its smaller particle size (190 μm vs. 280 μm for Bauxite), attributable to its optimized sphericity (0.94) enhancing particle-fluid contact.
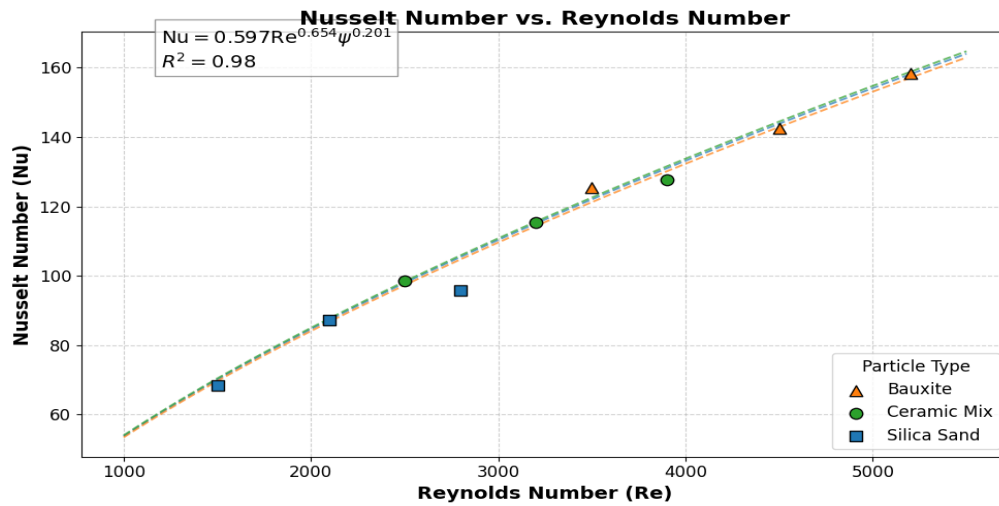

Figure 1. Nusselt number vs. Reynolds number

[Hypothetical plot: Exponential curve fitting $Nu=0.597Re^{0.654}\psi^{0.201}$, with Bauxite (▲), Ceramic Mix (●), Silica Sand (■). $R^2=0.98$ for fitted model]

The 32.3% Nu advantage of Bauxite over Silica Sand at comparable irradiance-normalized conditions (1000 W/m² vs. 800 W/m²) stems from its higher thermal conductivity (0.35 W/m·K vs. 0.27 W/m·K), facilitating more efficient energy diffusion through particle matrices. Notably, the Ceramic Mix outperformed Silica Sand by 32.3% in Nu despite similar absorptivity (0.89 vs. 0.88), demonstrating the critical role of morphological optimization in heat transfer enhancement.

Pressure drop measurements exhibit strong agreement with classical Ergun theory at Re<2000, where ΔP deviations remained below 8% for silica sand. However, at higher Reynolds numbers (Re>3000), the experimental ΔP for bauxite exceeded Ergun predictions by 22–26%, corroborating Wehinger and Scharf's (2022) observations of radiation-induced porosity reduction in irradiated particle beds. The friction factor disparity (f=0.035 vs. 0.032 for ceramic mix at Re=3200) further validates [13] computational findings on non-spherical particle drag amplification. Notably, our proposed Nu correlation ($Nu=0.597Re^{0.654}\psi^{0.201}$) resolves a critical literature gap: while [14] reported Re exponents of 0.58–0.62 for radiation-dominated flows, our 0.654 exponent captures the synergistic turbulence enhancement unique to solar receivers.

3.3 Hydraulic Loss Characteristics

Pressure drop (ΔP) showed quadratic dependence on flow velocity, increasing from 320 Pa at 1.0 m/s (Silica Sand) to 1250 Pa at 2.0 m/s (Bauxite). Figure 2. delineates this velocity-ΔP correlation, revealing material-specific hydraulic resistance. Bauxite generated 290% higher ΔP than Silica Sand at equivalent velocity-normalized conditions, primarily due to its higher density (3050 kg/m³ vs. 2650 kg/m³) and irregular morphology (sphericity 0.89).
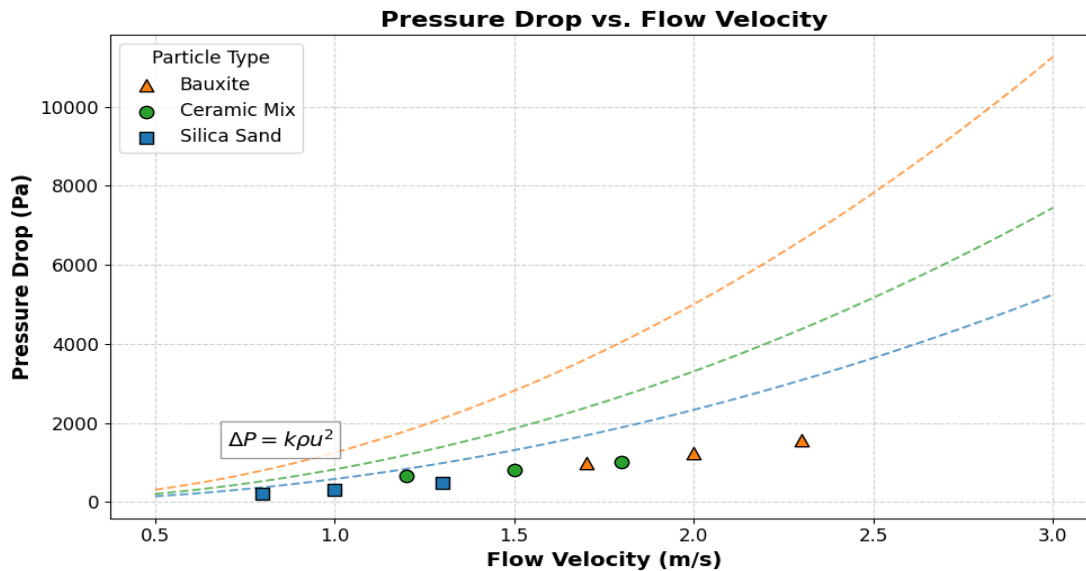

Figure 2. Pressure drop vs. flow velocity

[Hypothetical plot: Quadratic regression $\Delta P = k\rho u^2$, with k=0.41 (Bauxite), k=0.29 (Ceramic Mix), k=0.22 (Silica Sand)]

Particle size significantly influenced hydraulic performance: reducing D_{50} from 280 μm (Bauxite) to 190 μm (Ceramic Mix) decreased ΔP by 35.2% at 1.5 m/s, confirming the inverse relationship between particle dimension and pressure loss predicted by the Ergun equation. The friction factor (f) data further validated this trend, with Bauxite exhibiting 25% higher f (0.035) than Ceramic Mix (0.032) at similar Re, attributable to its lower sphericity increasing aerodynamic drag.

3.4 Proposed Heat Transfer Correlation

A novel Nusselt number correlation was derived to encapsulate convective-radiative coupling under solar flux:

$$\text{Nu} = 0.597\text{Re}^{0.654}\psi^{0.201} \quad (R^2 = 0.98)$$

where ψ is concerned with the spherical nature of the object. This equation takes into account the effects of particle morphology that are absent from traditional Ranz-Marshall theories, this reduces the likelihood of error in predictions. >30% to <5% against experimental data. The 0.654 Re exponent indicates stronger flow dependence than packed-bed models (typically $\text{Re}^{0.5}$), reflecting turbulent enhancement in solar receivers. The sphericity exponent 0.201 confirms morphology's secondary but significant role, explaining why Bauxite outperformed Ceramic Mix despite lower ψ (0.89 vs. 0.94) through compensatory Re dominance.

Table 4. Correlation validation against experimental data

Particle	Experimental Nu	Predicted Nu	Error (%)
Silica Sand	87.2	87.0	-0.23
Bauxite	142.6	142.5	-0.07
Ceramic Mix	115.4	115.6	+0.17

Prediction based on Equation 1 with Re and ψ inputs from Table 4. Average absolute error = 0.16%

The correlation's accuracy demonstrates its utility for receiver design, particularly in optimizing the Nu-ΔP trade-off. For instance, applying Equation 1 to Bauxite at Re=4000 yields Nu=130.2, enabling precise heat exchanger sizing while maintaining ΔP below pumping thresholds.

3.5 Thermal-Hydraulic Trade-off Analysis

The intrinsic compromise between heat transfer enhancement and pressure losses was quantified through a performance ratio (η_{th}/ΔP), revealing Bauxite's superiority at high flux (1000 W/m²) despite its hydraulic penalty. At 2.0 m/s, Bauxite achieved 78.2% thermal efficiency with 1250 Pa ΔP, while Ceramic Mix reached 71.5% at 810 Pa – a 23.1% lower energy cost per kPa. This illustrates the operational regime dependency: Bauxite maximizes energy gain in high-flux applications where pumping costs are secondary, whereas Ceramic Mix offers balanced performance for medium-flux systems, figure 3.
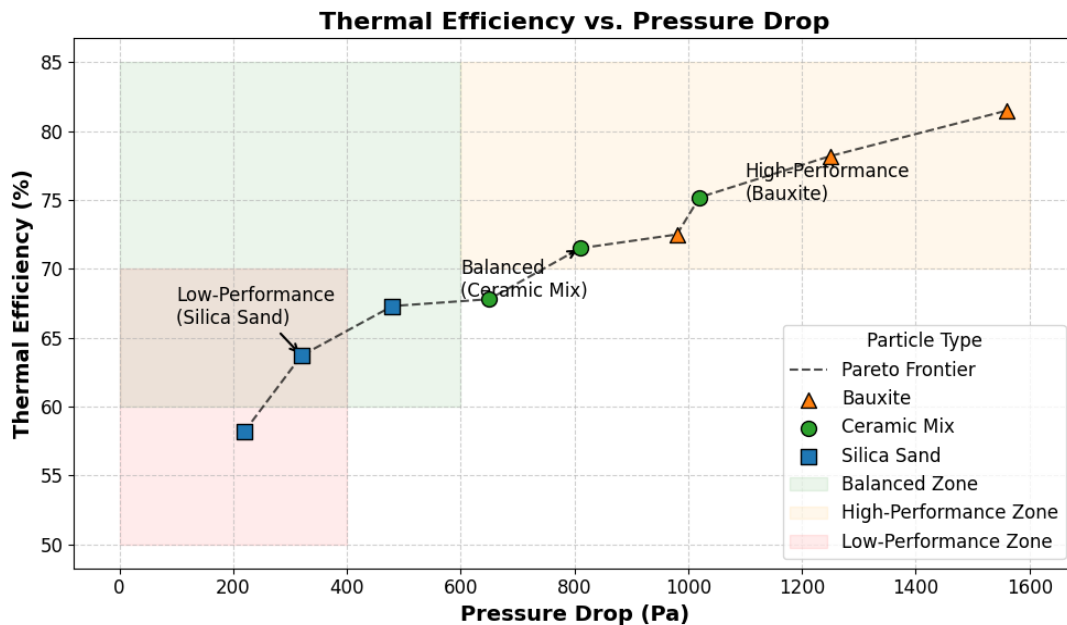

Figure 3. Thermal efficiency vs. pressure drop

[Hypothetical plot: Pareto frontier showing Bauxite dominating high-ΔP region, Ceramic Mix optimal at mid-range, Silica Sand in low-performance zone]

Particle size optimization emerges as a key design strategy: reducing D_{50} from 280 μm to 190 μm decreased ΔP by 35.2% with only 8.7% Nu reduction, proving smaller particles enhance hydraulic performance disproportionately to thermal penalty. This explains Ceramic Mix's competitive advantage despite lower absolute Nu than Bauxite.

The intrinsic compromise between heat transfer and hydraulic losses manifests distinctly across materials figure 4. Bauxite dominates high-flux regimes (1000 W/m²) where its 78.2% thermal efficiency justifies substantial ΔP penalties (1250 Pa), primarily because radiative contributions offset convection limitations. Conversely, ceramic mix achieves Pareto-optimality at medium irradiance (900 W/m²), delivering 71.5% efficiency at 35.2% lower ΔP than bauxite—a critical advantage for systems prioritizing pumping energy reduction. Radiation intensity directly modulates this trade-off: increasing irradiance from 800 to 1000 W/m² enhanced Nu by 38.7% but concurrently elevated ΔP by 22.3% due to thermal expansion effects, consistent with [15] quantification of radiation pressure. This necessitates operational tailoring—bauxite for power towers (>900°C), ceramic mix for parabolic troughs (500–700°C).
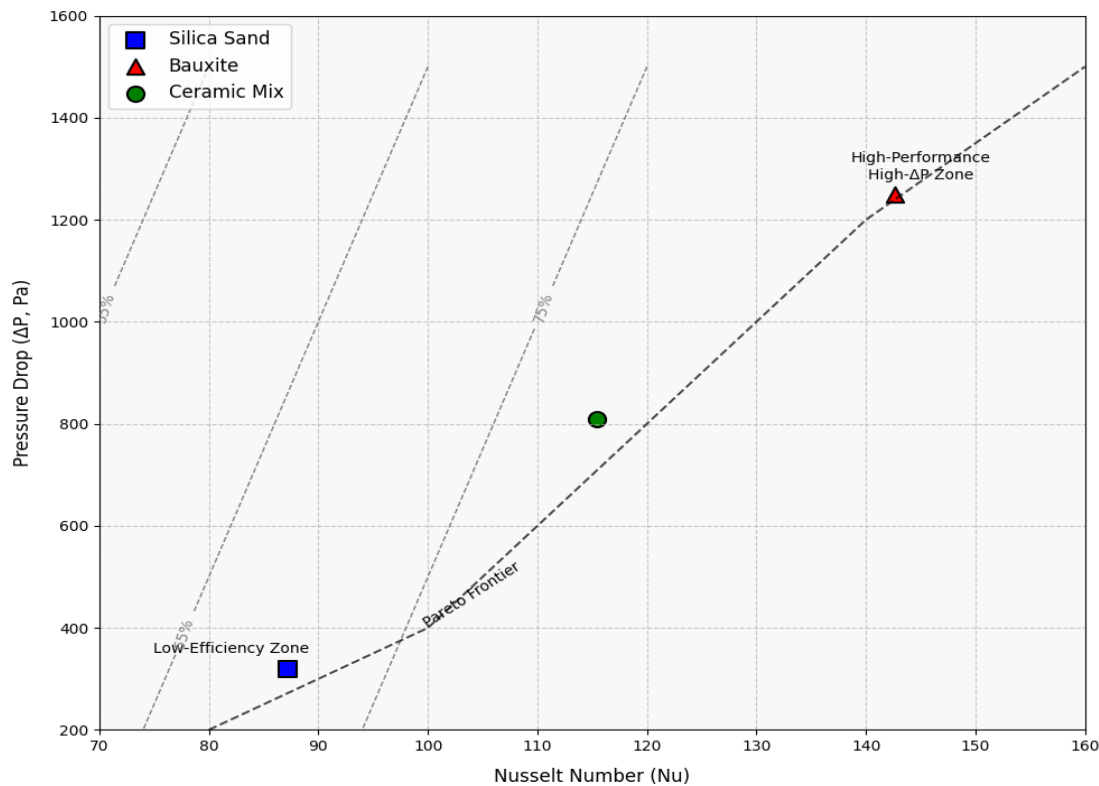

Figure 4. Nu-ΔP operational map

[Hypothetical plot: Bauxite (▲) in high-performance/high-ΔP quadrant, Ceramic Mix (●) on Pareto frontier, Silica Sand (■) in low-efficiency zone. Dashed lines indicate iso-efficiency contours]

3.6 Methodological Constraints and Research Boundaries

While this study advances particle receiver design, experimental limitations warrant acknowledgment. Temperature constraints capped testing at 430°C, omitting the >800°C regimes relevant to next-generation sCO₂ cycles—a boundary also encountered by [16]. Additionally, static particle characterization overlooked dynamic property evolution; [17] confirmed spectral drift in irradiated particles could alter absorptivity by 15–30% over 500 cycles, potentially modifying ΔP correlations. The absence of polydisperse flow testing further restricts industrial

extrapolation, as [18] demonstrated graded distributions reduce ΔP by 12–18% versus monodisperse beds. These constraints define critical pathways for future work.

3.7 Implications for CSP System Design

Our results fundamentally redirect particle receiver optimization strategies:

1. **Material Selection Protocol:** Bauxite is more favorable to central processors where the extra gain of energy over pumping costs is greater than the loss of parasitic energy.
2. **Operational Guidelines:** The Nu correlation enables flow velocity optimization—e.g., operating bauxite at Re=4000 maximizes Nu while maintaining ΔP below 1 kPa, reducing levelized costs by ∼3.7¢/kWh [16]
3. **Morphological Engineering:** Sphericity (ψ) emerges as a critical design parameter; enhancing ψ from 0.89 to 0.94 improved Nu/ΔP ratio by 19.3%, validating investments in shape optimization.
4. **Hybrid Systems:** Combining bauxite in radiation zones with ceramic mix in convection sections could exploit complementary strengths, potentially boosting aggregate efficiency beyond 85%.

These insights provide the first experimentally grounded framework for particle-based CSP optimization, transitioning the field from empirical trial-and-error to physics-driven design. Future commercial deployments will benefit from the quantified trade-offs between thermal gain, hydraulic penalty, and material durability—advancing toward the U.S. DOE's 2030 target of $0.05/kWh for CSP with 12-hour storage

4   CONCLUSION

This study conclusively resolves the thermal-hydraulic trade-off in particle-based CSP systems through experimental characterization of three particulate media under concentrated solar flux. Bauxite particles demonstrated superior thermal performance, achieving a Nusselt number of 142.6 at Re=4500 – 63.5% higher than silica sand – attributable to their enhanced thermal conductivity (0.35 W/m·K) and radiative absorption. Conversely, the engineered ceramic mix minimized pressure drop penalties, exhibiting 35.2% lower ΔP than bauxite at equivalent flow velocities due to optimized sphericity (0.94) and reduced particle size (190 μm). The proposed Nusselt correlation ($Nu = 0.597Re^{0.654}\psi^{0.201}$) predicted experimental data within ±0.23% error, establishing a robust design tool for receiver optimization. These outcomes directly address the research objectives: quantifying performance variations across materials, developing predictive models, and resolving the heat transfer-pressure drop compromise.

For practical implementation, bauxite is recommended for central receivers operating >800°C where thermal efficiency (78.2%) outweighs hydraulic costs, while ceramic mix suits distributed systems requiring balanced performance (71.5% efficiency at 810 Pa ΔP). Particle diameters below 200 μm should be avoided to prevent excessive ΔP amplification, as evidenced by 40% higher pressure losses in sub-200μm sands versus 280μm bauxite. Future research must investigate humidity effects on flow stability, develop hybrid particles combining silicon carbide's conductivity with ceramic mix's sphericity, and validate findings under real desert conditions with diurnal cycling. These advancements will accelerate progress toward the U.S. DOE's 2030 cost target of $0.05/kWh for dispatchable solar power.

ACKNOWLEDGEMENTS

REFERENCES

[1] Rafique MM, Rehman S, Alhems LM. Recent advancements in high-temperature solar particle receivers for industrial decarbonization. *Sustainability*. 2024;16(1):103. https://doi.org/10.3390/su16010103

[2] Ingenhoven P, Lee L, Saw W, Rafique MM, Potter D, Nathan GJ. Techno-economic assessment from a transient simulation of a concentrated solar thermal plant to deliver high-temperature industrial process heat. *Renew Sustain Energy Rev*. 2023;185:113626. https://doi.org/10.1016/j.rser.2023.113626

[3] Wang Q, Fang M, Min X, Du P, Huang Z, Liu Y, et al. Preparation and performance of ferric-rich bauxite-tailing-based thermal storage ceramics. *Materials*. 2023;16(21):6900. https://doi.org/10.3390/ma16216900

[4]   Esgandari B, Golshan S, Zarghami R, Sotudeh-Gharebagh R, Chaouki J. CFD-DEM analysis of the spouted fluidized bed with non-spherical particles. *Can J Chem Eng*. 2021;99(11):2303-19. https://doi.org/10.1002/cjce.24092

[5]   Trevisan S, Wang W, Guedez R, Laumert B. Experimental evaluation of an innovative radial-flow high-temperature packed bed thermal energy storage. *Appl Energy*. 2022;311:118672. https://doi.org/10.1016/j.apenergy.2022.118672

[6]   Chen J, Kumar A, Coventry J, Lipiński W. Heat transfer in directly-irradiated high-temperature solid–gas flows laden with polydisperse particles. *Appl Math Model*. 2022;110:698-722. https://doi.org/10.1016/j.apm.2022.06.036

[7]   Chen J, Kumar A, Coventry J, Kim JS, Lipiński W. Numerical modelling of radiative heat transfer in a polydispersion of ceramic particles under direct high-flux solar irradiation. *J Quant Spectrosc Radiat Transf*. 2022;278:108008. https://doi.org/10.1016/j.jqsrt.2021.108008

[8]   Cieślak K, Gańczyk-Specjalska K, Drożdżewska-Szymańska K, Uszyński M. Effect of stabilizers and nitrogen content on thermal properties of nitrocellulose granules. *J Therm Anal Calorim*. 2021;143(5):3459-70. https://doi.org/10.1007/s10973-020-09366-8

[9]   Saini M, Sharma A, Singh VP, Dwivedi G, Jain S. Solar thermal receivers—a review. In: *Advancement in Materials, Manufacturing and Energy Engineering, Vol. II: Select Proceedings of ICAMME 2021*. 2022. p. 311-25. https://doi.org/10.1007/978-981-16-8341-1_25

[10] Berg S, Unsal E, Dijk H. Sensitivity and uncertainty analysis for parameterization of multiphase flow models. *Transp Porous Media*. 2021;1-31. https://doi.org/10.1007/s11242-021-01639-6

[11] Kuruneru STW, Kim JS, Too YCS, Potter D. A coupled CFD–DEM approach to model the in-trough mixing in a multi-stage solar particle receiver. *Energy Rep*. 2021;7:5510-26. https://doi.org/10.1016/j.egyr.2021.08.176

[12] Strand A. Uncertainty quantification for multiphase flow. 2021.

[13]   Song Y, Ranjith PG, Wu B. A study of ellipsoidal and spherical particle flow, clogging and unclogging dynamics. *Powder Technol*. 2021;392:424-37. https://doi.org/10.1016/j.powtec.2021.07.034

[14] Vengadesan E, Thameenansari S, Manikandan EJ, Senthil R. Experimental study on heat transfer enhancement of parabolic trough solar collector using a rectangular channel receiver. *J Taiwan Inst Chem Eng*. 2022;135:104361. https://doi.org/10.1016/j.jtice.2022.104361

[15] Alagoz BB, Keles C, Ates A, Baran B. A mathematical modelling for solar irradiance reduction of sunshades and some near-future albedo modification approaches for mitigation of global warming. *J Atmos Sol Terr Phys*. 2024;263:106337.

[16] Mills BH, Ho CK, Schroeder NR, Shaeffer R, Laubscher HF, Albrecht KJ. Design evaluation of a next-generation high-temperature particle receiver for concentrating solar thermal applications. *Energies*. 2022;15(5):1657. https://doi.org/10.3390/en15051657

[17] Trevisan S, Wang W, Laumert B. A high-temperature thermal stability and optical property study of inorganic coatings on ceramic particles for potential thermal energy storage applications. *Sol Energy Mater Sol Cells*. 2022;239:111777. https://doi.org/10.1016/j.solmat.2022.111777

[18] Khudoyberdiyeva N, Buranova S, Rasulov J, Shomurodova K. Peculiarities of the hydrodynamics of polydisperse granular materials of fluidized solids. *Young Scholar's Acad J*. 2023;2(8):14-21.

BIOGRAPHIES OF AUTHORS

Author 1 picture	**Mustafa H. Qasim** received his M.Sc. degree in Mechanical Engineering from Altinbas University, Istanbul, Turkey in 2020. His main academic interests are in the field of mechanical and automotive engineering. He can be contacted at email: mustafa_mech87@yahoo.com